Available online at www.sciencedirect.com

ScienceDirect

Solar Energy 105 (2014) 455–467

SOLAR ENERGY

www.elsevier.com/locate/solener

Semi-empirical relation for forced convective analysis through a solar collector

Rehena Nasrin *, M.A. Alim

Department of Mathematics, Bangladesh University of Engineering & Technology, Dhaka 1000, Bangladesh

Received 25 July 2013; received in revised form 17 September 2013; accepted 27 March 2014
Available online 6 May 2014

Communicated by: Associate Editor Brian Norton

Abstract

A numerical study has been conducted to investigate the forced convection through a flat plate solar collector. The water alumina nanofluid is used as the working fluid inside the riser pipe of the solar collector. The governing differential equations with boundary conditions are solved by finite element method using Galerkin's weighted residual scheme. The effects of major system parameters on the forced convection heat transfer are simulated. These parameters include the the Reynolds number (*Re*) and Prandtl number (*Pr*). Comprehensive average Nusselt number, average temperature, mean velocity, percentage of collector efficiency, mid-height temperature for both nanofluid and base fluid through the collector pipe are presented as functions of the governing parameters mentioned above. The numerical results show that the highest heat loss rate is observed for both the largest *Re* and *Pr*. Percentage of collector efficiency enhances for growing *Re* and falling *Pr*. A correlation is developed among average Nusselt number, Reynolds number and Prandtl number. Then a semi-empirical relation is established from this correlation with experimental data found in the literature.

Keywords: Forced convection; Flat plate solar collector; Finite element method; Water-Al_2O_3 nanofluid; Semi-empirical relation

1. Introduction

The flat-plate solar collector is commonly used today for the collection of low temperature solar thermal energy. It is used for solar water-heating systems in homes and solar space heating. Because of the desirable environmental and safety aspects it is widely believed that solar energy should be utilized instead of other alternative energy forms, even when the costs involved are slightly higher. Solar collectors are key elements in many applications, such as building heating systems, solar drying devices, etc. Solar energy has the greatest potential of all the sources of renewable energy especially when other sources in the country have depleted. The fluids with solid-sized nanoparticles suspended in them are called "nanofluids." Applications of nanoparticles in thermal field are to enhance heat transfer from solar collectors to storage tanks, to improve efficiency of coolants in transformers. The sun is a sphere of intensely hot gaseous matter with a diameter of 1.39×10^9 m. The solar energy strikes our planet a mere 8 min and 20 s after leaving the giant furnace. The sun has an effective blackbody temperature of 5762 K.

Sandhu (2013) experimentally studied temperature field in flat-plate collector and heat transfer enhancement with the use of insert devices. Various new configurations of the conventional insert devices were tested over a wide range of Reynolds number (200–8000). Comparison of these devices showed that in laminar flow regime, wire mesh proved to be an effective insert device and enhanced

* Corresponding author. Tel.: +880 01913583407.
E-mail address: rehena@math.buet.ac.bd (R. Nasrin).

http://dx.doi.org/10.1016/j.solener.2014.03.035
0038-092X/

Nomenclature

A	surface area of the collector (m^2)
C_p	specific heat at constant pressure ($J\ kg^{-1}\ K^{-1}$)
h	local heat transfer coefficient ($W\ m^{-2}\ K^{-1}$)
I	intensity of solar radiation ($W\ m^{-2}$)
k	thermal conductivity ($W\ m^{-1}\ K^{-1}$)
L	length of the riser pipe (m)
m	mass flow rate ($Kg\ s^{-1}$)
Nu	Nusselt number, $Nu = hL/k_f$
Pr	Prandtl number, $Pr = \nu_f/\alpha_f$
Re	Reynolds number, $Re = \frac{U_{in}L}{\nu_f}$
T	dimensional temperature (K)
T_{in}	input temperature of fluid (K)
T_{out}	output temperature of fluid (K)
u, v	dimensional x and y components of velocity ($m\ s^{-1}$)
U, V	dimensionless velocities, $U = \frac{u}{U_{in}}$, $V = \frac{v}{U_{in}}$
U_i	input velocity of fluid ($m\ s^{-1}$)
X, Y	dimensionless coordinates, $X = x/L$, $Y = y/L$
x, y	dimensional coordinates (m)

Greek symbols

α	fluid thermal diffusivity ($m^2\ s^{-1}$)
β	thermal expansion coefficient (K^{-1})
ϕ	nanoparticles volume fraction
ν	kinematic viscosity ($m^2\ s^{-1}$)
η	collector efficiency, $\eta = \frac{mC_p(T_{out}-T_{in})}{AI}$
θ	dimensionless temperature, $\theta = (T - T_{in})/(T_{col} - T_{in})$
ρ	density ($kg\ m^{-3}$)
μ	dynamic viscosity ($N\ s\ m^{-2}$)
V	dimensionless velocity field

Subscripts

av	average
c	collector
f	fluid
nf	nanofluid
s	solid particle

Nusselt number by 270% while in turbulent flow regime. While in Reynolds number range 2700–8000, concentric coil insert significantly increased the heat transfer and an increase of 460% in Nusselt number was witnessed. Martín et al. (2011) also analyzed experimental heat transfer research in enhanced flat-plate solar collectors. To test the enhanced solar collector and compare with a standard one, an experimental side-by-side solar collector test bed was designed and constructed. Modeling of flat-plate solar collector operation in transient states was conducted by Saleh (2012). This study presents a one-dimensional mathematical model for simulating the transient processes which occur in liquid flat-plate solar collectors. The proposed model simulated the complete solar collector system including the flat-plate and the storage tank.

Azad (2009) investigated interconnected heat pipe solar collector. Performance of a prototype of the heat pipe solar collector was experimentally examined and the results were compared with those obtained through theoretical analysis. Zambolin (xxxx) theoretically and experimentally performed solar thermal collector systems and components. Testing of thermal efficiency and optimization of these solar thermal collectors were addressed and discussed in this work. Piao (1994) studied forced convective heat transfer in cross-corrugated solar air heaters. Kolb (1999) experimentally studied solar air collector with metal matrix absorber. Nag et al. (1989) analyzed parametric study of parallel flow flat plate solar collector using finite element method. Lund (1986) analyzed general thermal behavior of parallel-flow flat-plate solar collector absorbers. Tripanagnostopoulos et al. (2000) investigated solar collectors with colored absorbers.

Mahian et al. (2013) performed a review of the applications of nanofluids in solar energy. The effects of nanofluids on the performance of solar collectors and solar water heaters from the efficiency, economic and environmental considerations viewpoints and the challenges of using nanofluids in solar energy devices were discussed. Enhancement of flat-plate solar collector thermal performance with silver nano-fluid was conducted by Polvongsri and Kiatsiriroat (2011). With higher thermal conductivity of the working fluid the solar collector performance could be enhanced compared with that of water. The solar collector efficiency with the nano-fluid was still high even the inlet temperature of the working fluid was increased. Natarajan and Sathish (2009) studied role of nanofluids in solar water heater. Heat transfer enhancement in solar devices is one of the key issues of energy saving and compact designs. The aim of this paper was to analyze and compare the heat transfer properties of the nanofluids with the conventional fluids. Struckmann et al. (2008) analyzed flat-plate solar collector where efforts had been made to combine a number of the most important factors into a single equation and thus formulate a mathematical model which would describe the thermal performance of the collector in a computationally efficient manner.

Generally a direct absorption solar collector (DAC) using nanofluids as the working fluid performs better than a flat-plate collector. Much better designed flat-plate collectors might be able to match a nanofluid based DAC under certain conditions. Tyagi et al. (2009) investigated Predicted efficiency of a low-temperature nanofluid-based direct absorption solar collector. It was observed that the presence of nanoparticles increased the absorption of

incident radiation by more than nine times over that of pure water. According to the results obtained from this study, under similar operating conditions, the efficiency of a DAC using nanofluid as the working fluid was found to be up to 10% higher than that of a flat-plate collector. Kazeminejad (2002) numerically analyzed two dimensional parallel flow flat-plate solar collectors. Temperature distribution over the absorber plate of a parallel flow flat-plate solar collector was analyzed with one- and two-dimensional steady-state conduction equations with heat generations.

Otanicar et al. (2010) studied nanofluid-based direct absorption solar collector. They reported on the experimental results on solar collectors based on nanofluids made from a variety of nanoparticles carbon nanotubes, graphite, and silver. They demonstrated efficiency improvements of up to 5% in solar thermal collectors by utilizing nanofluids as the absorption mechanism. In addition the experimental data were compared with a numerical model of a solar collector with direct absorption nanofluids. Karanth et al. (2011) performed numerical simulation of a solar flat plate collector using discrete transfer radiation model (DTRM)–a CFD Approach. Dynamics (CFD) by employing conjugate heat transfer showed that the heat transfer simulation due to solar irradiation to the fluid medium, increased with an increase in the mass flow rate. Also it was observed that the absorber plate temperature decreased with increase in the mass flow rate. Karuppa et al. (2012) experimentally investigated a new solar flat plate collector. Experiments had been carried out to test the performance of both the water heaters under water circulation with a small pump and the results were compared. The results showed that the system could reach satisfactory levels of efficiency.

Dara et al. (2013) conducted evaluation of a passive flat-plate solar collector. The research investigated the variations of top loss heat transfer coefficient with absorber plate emittance; and air gap spacing between the absorber plate and the cover plate. Amrutkar and Ghodke (2012) studied solar flat plate collector analysis. The objective of their study was to evaluate the performance of FPC with different geometric absorber configuration. It was expected that with the same collector space higher thermal efficiency or higher water temperature could be obtained. Iordanou (2009) investigated flat-plate solar collectors for water heating with improved heat Transfer for application in climatic conditions of the mediterranean region. The aim of this research project was to improve the thermal performance of passive flat plate solar collectors using a novel cost effective enhanced heat transfer technique. This work focused on the process of energy conversion from the collector to the working fluid. This was accomplished by employing an aluminum grid placed in the channels of a collector to induce a gradient of heat capacitance.

Álvarez et al. (2010) studied finite element modeling of a solar collector. A mathematical model of a serpentine flat-plate solar collector using finite elements was presented. The numerical simulations focused on the thermal and hydrodynamic behavior of the collector. Conduction convection radiation processes of a solar collector using FEA was performed by Moningi (2009). Radiation dominated the other two processes. It being non-linear phenomena required an iterative procedure to solve problems analytically, which was quite difficult. So, he tried to find the temperature distribution of the solar collector using FEA. Lambert and Cuevas (2006) conducted Enhanced heat transfer using oscillatory flows in solar collectors. They proposed the use of oscillatory laminar flows to enhance the transfer of heat from solar collectors. The idea was to explore the possibility of transferring the heat collected from a solar device to a storage tank by means of a zero-mean oscillating fluid contained in a tube. Selected nanofluids might improve the efficiency of direct absorption solar thermal collectors. To determine the effectiveness of nanofluids in solar applications, their ability to convert light energy to thermal energy must be known. That is, their absorption of the solar spectrum must be established.

Taylor et al. (2011) analyzed nanofluid optical property characterization: towards efficient direct absorption solar collectors. Their study compared model predictions to spectroscopic measurements of extinction coefficients over wavelengths that were important for solar energy (0.25–2.5 μm). Chabane et al. (2013) studied thermal performance optimization of a flat plate solar air heater. Experimentally investigates of single pass solar air heater without fins; present the aims to review of designed and analyzed a thermal efficiency of flat-plate solar air heaters. The received energy and useful energy rates of the solar air heaters were evaluated for various air flow rates were (0.0108, 0.0145, 0.0161, 0.0184 and 0.0203 $kg\,s^{-1}$) are investigated. Optimum values of air mass flow rates were suggested maximizing the performance of the solar collector.

In the light of above discussions, it is seen that there has been a good number of works in the field of heat loss system through a flat plate solar collector. In spite of that there is some scope to work with fluid flow, heat loss and enhancement of collector efficiency using nanofluid. Also temperature, streamfunction and heatfunction profile through the riser pipe of the collector cannot be shown in any experimental woks.

In this paper, we investigate numerically the forced convection flow through the riser pipe of a flat plate solar collector. The objective of this paper is to present temperature, streamfunction and heatfunction profile as well as heat loss system used to harness solar energy. In addition a correlation among *Nu*, *Re* and *Pr* is developed. Then a semi-empirical relation is established with the experimental data of Sandhu (Sandhu, 2013).

2. Problem formulation

A cross section of the system considered in the present study is shown in Fig. 1. The system consists of a flat plate

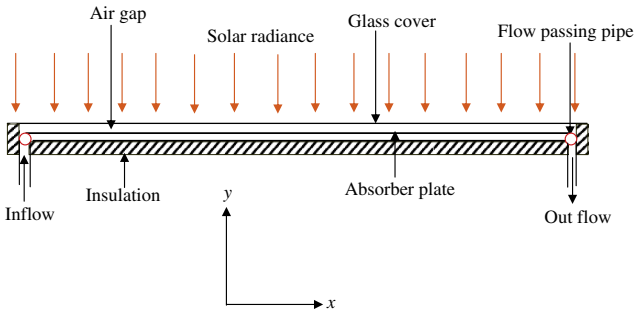

Fig. 1. Schematic diagram of the solar collector.

solar collector. The fluid through the copper riser pipe is water-based nanofluid containing Al_2O_3 nanoparticles. The nanofluid is assumed incompressible and the flow is considered to be laminar. It is taken that water and nanoparticles are in thermal equilibrium and no slip occurs between them. The flat-plate solar collector is an insulated metal box with a glass cover (called the glazing) and a dark-colored absorber plate. A, L and D are the surface area of the collector, length and inner diameter of the riser pipe. The density of the nanofluid is approximated by the Boussinesq model. Only steady state case is considered. The computation domain is a fluid passing copper riser pipe which is attached ultrasonically to the absorber plate.

It is necessary to measure its thermal performance, i.e. the useful energy gain or the collector efficiency. If I is the intensity of solar radiation, incident on the aperture plane of the solar collector having a collector surface area of A, then the amount of solar radiation received by the collector is:

$$Q_i = I.A \tag{1}$$

However, a part of this radiation is reflected back to the sky, another component is absorbed by the glazing and the rest is transmitted through the glazing and reaches the absorber plate as short wave radiation.

Therefore the conversion factor indicates the percentage of the solar rays penetrating the transparent cover of the collector (transmission) and the percentage being absorbed. Basically, it is the product of the rate of transmission of the cover (λ) and the absorption rate of the absorber (κ). Thus,

$$Q_{recv} = I(\lambda\kappa)A \tag{2}$$

As the collector absorbs heat its temperature is getting higher than that of the surrounding and heat is lost to the atmosphere by convection and radiation. The rate of heat loss (Q_{loss}) depends on the collector overall heat transfer coefficient (h) and the collector temperature.

$$Q_{loss} = hA(T_{col} - T_{amb}) \tag{3}$$

Thus, the rate of useful energy extracted by the collector (Q_{usfl}), expressed as a rate of extraction under steady state conditions, is proportional to the rate of useful energy absorbed by the collector, less the amount lost by the collector to its surroundings. This is expressed as follows:

$$Q_{usfl} = Q_{recv} - Q_{loss} = I(\lambda\kappa)A - hA(T_{col} - T_{amb}) \tag{4}$$

where T_{col} and T_{amb} are collector temperature and ambient temperature outside the collector respectively. It is also known that the rate of extraction of heat from the collector may be measured by means of the amount of heat carried away in the fluid passed through it, that is:

$$Q_{usfl} = mC_p(T_{out} - T_{in}) \tag{5}$$

A measure of a flat plate collector performance is the collector efficiency (η) defined as the ratio of the useful energy gain (Q_{usfl}) to the incident solar energy over a particular time period:

$$\eta = \frac{\text{useful gain}}{\text{available energy}} = \frac{mC_p(T_{out} - T_{in})}{AI} \tag{6}$$

where m is the mass flow rate of the fluid flowing through the collector; C_p is the specific heat at constant pressure and T_{in} and T_{out} are the mean fluid inlet and outlet temperatures, respectively.

The governing equations for laminar forced convection through a solar collector filled with water-alumina nanofluid in terms of the Navier–Stokes and energy equation (dimensional form) are given as:

Continuity equation:

$$\frac{\partial u}{\partial x} + \frac{\partial v}{\partial y} = 0 \tag{7}$$

x-momentum equation:

$$\rho_{nf}\left(u\frac{\partial u}{\partial x} + v\frac{\partial u}{\partial y}\right) = -\frac{\partial p}{\partial x} + \mu_{nf}\left(\frac{\partial^2 u}{\partial x^2} + \frac{\partial^2 u}{\partial y^2}\right) \tag{8}$$

y-momentum equation:

$$\rho_{nf}\left(u\frac{\partial v}{\partial x} + v\frac{\partial v}{\partial y}\right) = -\frac{\partial p}{\partial y} + \mu_{nf}\left(\frac{\partial^v}{\partial x^2} + \frac{\partial^2 v}{\partial y^2}\right) \tag{9}$$

Energy equation:

$$u\frac{\partial T}{\partial x} + v\frac{\partial T}{\partial y} = \alpha_{nf}\left(\frac{\partial^2 T}{\partial x^2} + \frac{\partial^2 T}{\partial y^2}\right) \tag{10}$$

where, $\rho_{nf} = (1-\phi)\rho_f + \phi\rho_s$ is the density,

$(\rho C_p)_{nf} = (1-\phi)(\rho C_p)_f + \phi(\rho C_p)_s$ is the heat capacitance,

$\alpha_{nf} = k_{nf}/(\rho C_p)_{nf}$ is the thermal diffusivity,

In the current study, the viscosity of the nanofluid is considered by the Pak and Cho correlation (Pak and Cho, 1998). This correlation is given as

$$\mu_{nf} = \mu_f(1 + 39.11\phi + 533.9\phi^2) \tag{11}$$

and the thermal conductivity of Maxwell Garnett (MG) model Maxwell-Garnett, 1904 is

$$k_{nf} = k_f\frac{k_s + 2k_f - 2\phi(k_f - k_s)}{k_s + 2k_f + \phi(k_f - k_s)} \tag{12}$$

The boundary conditions are:

at all solid boundaries: $u = v = 0$

at the solid surfaces of the pipe: inward heat flux $q = I(\lambda\kappa)A - hA(T_{col} - T_{amb})$
at the inlet boundary: $T = T_{in}$, $u = U_{in}$
at the outlet boundary: convective boundary condition $p = 0$.

The above equations are non-dimensionalized by using the following dimensionless dependent and independent variables:

$$X = \frac{x}{L}, Y = \frac{y}{L}, U = \frac{u}{U_{\text{in}}}, V = \frac{v}{U_{\text{in}}}, P = \frac{p}{\rho_f U_{\text{in}}^2}, \theta = \frac{(T - T_{\text{in}})k_f}{\text{q}}$$

Then the non-dimensional governing equations are

$$\frac{\partial U}{\partial X} + \frac{\partial V}{\partial Y} = 0 \tag{13}$$

$$U\frac{\partial U}{\partial X} + V\frac{\partial U}{\partial Y} = -\frac{\rho_f}{\rho_{nf}}\frac{\partial P}{\partial X} + \frac{v_{nf}}{v_f}\frac{1}{Re}\left(\frac{\partial^2 U}{\partial X^2} + \frac{\partial^2 U}{\partial Y^2}\right) \tag{14}$$

$$U\frac{\partial V}{\partial X} + V\frac{\partial V}{\partial Y} = -\frac{\rho_f}{\rho_{nf}}\frac{\partial P}{\partial Y} + \frac{v_{nf}}{v_f}\frac{1}{Re}\left(\frac{\partial^2 V}{\partial X^2} + \frac{\partial^2 V}{\partial Y^2}\right) \tag{15}$$

$$U\frac{\partial \theta}{\partial X} + V\frac{\partial \theta}{\partial Y} = \frac{1}{RePr}\frac{\alpha_{nf}}{\alpha_f}\left(\frac{\partial^2 \theta}{\partial X^2} + \frac{\partial^2 \theta}{\partial Y^2}\right) \tag{16}$$

where $Pr = \frac{v_f}{\alpha_f}$ is the Prandtl number, $Re = \frac{U_{in}L}{v_f}$ is the Reynolds number.

The corresponding boundary conditions take the following form:

at all solid boundaries: $U = V = 0$
at the solid walls: $\frac{\partial \theta}{\partial Y} = -1$
at the inlet boundary: $\theta = 0$, $U = 1$
at the outlet boundary: convective boundary condition $P = 0$.

2.1. Average Nusselt number

The average Nusselt number (Nu) is expected to depend on a number of factors such as thermal conductivity, heat capacitance, viscosity, flow structure of nanofluids, volume fraction, dimensions and fractal distributions of nanoparticles. The non-dimensional form of local convective heat transfer at the top surface is

$$\overline{Nu} = -\frac{k_{nf}}{k_f}\frac{\partial \theta}{\partial Y}.$$

By integrating the local Nusselt number over the top heated surface, the average convective heat transfer along the heated wall of the collector is used by Saleh et al. (2011) as

$$Nu = \int_0^1 \overline{Nu}\, dX.$$

2.2. Mean bulk temperature and velocity

The mean bulk temperature and average sub domain velocity of the fluid inside the collector may be written as $\theta_{av} = \int \theta\, d\bar{V}/\bar{V}$ and $\mathrm{V}_{av} = \int \mathrm{V}\, d\bar{V}/\bar{V}$, where $\bar{V}$ is the volume of the collector.

2.3. Streamfunction

Streamfunction ψ is obtained from velocity components U and V. The relationships between stream function and velocity components is $U = \frac{\partial \psi}{\partial Y}$, $V = -\frac{\partial \psi}{\partial X}$.

Thus $$\frac{\partial^2 \psi}{\partial X^2} + \frac{\partial^2 \psi}{\partial Y^2} = \frac{\partial U}{\partial Y} - \frac{\partial V}{\partial X} \tag{17}$$

2.4. Heatfunction

Heatfunction ξ is obtained from conductive heat fluxes $(-\frac{\partial \theta}{\partial X}, -\frac{\partial \theta}{\partial Y})$ as well as convective heat fluxes $(U\theta, V\theta)$. It satisfies the steady energy balance equation such that $U\theta - \frac{\partial \theta}{\partial X} = \frac{\partial \xi}{\partial Y}$, $V\theta - \frac{\partial \theta}{\partial Y} = -\frac{\partial \xi}{\partial X}$.

Thus $$\frac{\partial^2 \xi}{\partial X^2} + \frac{\partial^2 \xi}{\partial Y^2} = \frac{\partial}{\partial Y}(U\theta) - \frac{\partial}{\partial X}(V\theta) \tag{18}$$

3. Numerical implementation

The Galerkin finite element method Taylor and Hood (1973) and Dechaumphai (1999) is used to solve the non-dimensional governing equations along with boundary conditions for the considered problem. The equation of continuity has been used as a constraint due to mass conservation and this restriction may be used to find the pressure distribution. The finite element method of Reddy and Gartling (1994) is used to solve the Eqs. (13)–(16), where the pressure P is eliminated by a constraint. The continuity equation is automatically fulfilled for large values of this constraint. Then the velocity components (U, V) and temperature (θ) are expanded using a basis set. The Galerkin finite element technique yields the subsequent nonlinear residual equations. Three points Gaussian quadrature is used to evaluate the integrals in these equations. The non-linear residual equations are solved using Newton–Raphson method to determine the coefficients of the expansions. The convergence of solutions is assumed when the relative error for each variable between consecutive iterations is recorded below the convergence criterion such that $|\psi^{n+1} - \psi^n| \leqslant 10^{-4}$, where n is the number of iteration and Ψ is a function of U, V and θ.

3.1. Mesh generation

In the finite element method, the mesh generation is the technique to subdivide a domain into a set of sub-domains, called finite elements, control volume, etc. The discrete

locations are defined by the numerical grid, at which the variables are to be calculated. It is basically a discrete representation of the geometric domain on which the problem is to be solved. The computational domains with irregular geometries by a collection of finite elements make the method a valuable practical tool for the solution of boundary value problems arising in various fields of engineering. Fig. 2 displays the finite element mesh of the present physical domain.

3.2. Grid independent test

An extensive mesh testing procedure is conducted to guarantee a grid-independent solution for $Re = 400$ and $Pr = 6.6$ in a solar collector. In the present work, we examine five different non-uniform grid systems with the following number of elements within the resolution field: 60, 240, 960, 3840 and 15360. The numerical scheme is carried out for highly precise key in the average Nusselt number for water-alumina nanofluid (= 5%) as well as base fluid (= 0%) for the aforesaid elements to develop an understanding of the grid fineness as shown in Table 2 and Fig. 3. The scale of the average Nusselt numbers for 3840 elements shows a little difference with the results obtained for the other elements. Hence, considering the non-uniform grid system of 3840 elements is preferred for the computation.

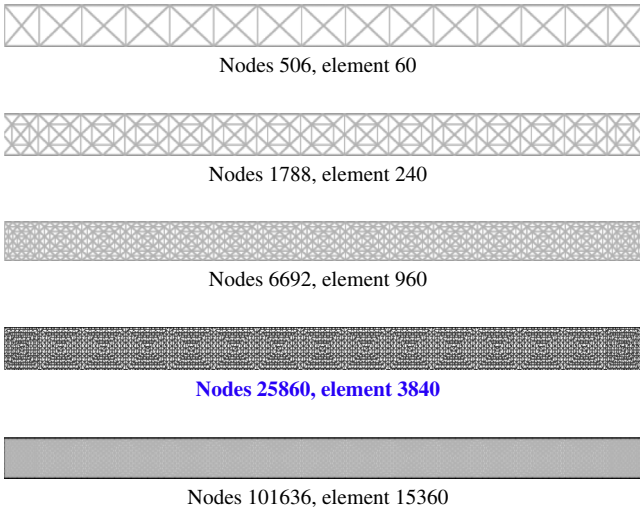

Fig. 2. Mesh generation of the riser pipe.

Table 1
Thermo physical properties of fluid and nanoparticles.

Physical properties	Fluid phase (Water)	Al_2O_3
C_p(J/kgK)	4179	765
ρ (kg/m^3)	997.1	3970
k (W/mK)	0.613	40
$\alpha \times 10^7$ (m^2/s)	1.47	131.7

Table 2
Grid Sensitivity Check at $Pr = 6.6$, $\phi = 5\%$ and $Re = 400$.

Nodes (elements)	506 (60)	1788 (240)	6692 (960)	25860 (3840)	101636 (15360)
Nu (nanofluid)	7.82945	9.19176	10.17518	10.84991	10.85001
Nu (basefluid)	6.62945	7.99976	8.88701	9.551698	9.551718
Time (s)	126.265	312.594	398.157	481.328	929.377

3.3. Thermo-physical properties

The thermo-physical properties of the nanoparticle are taken from Ogut (2009) and given in Table 1.

3.4. Code validation

The present numerical solution is validated by comparing the current code results for collector efficiency – temperature

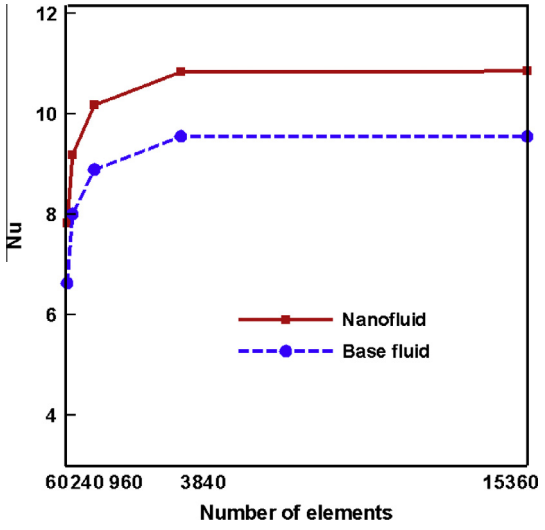

Fig. 3. Grid test for riser pipe of the solar collector.

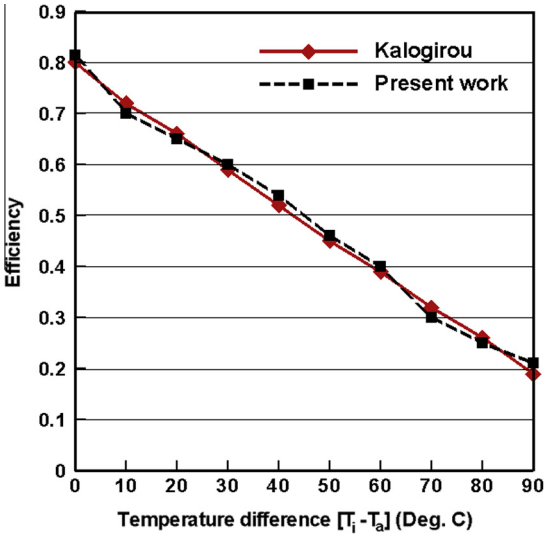

Fig. 4. Comparison between present code and Kalogirou (2004) at $I = 1000$ W/m^2.

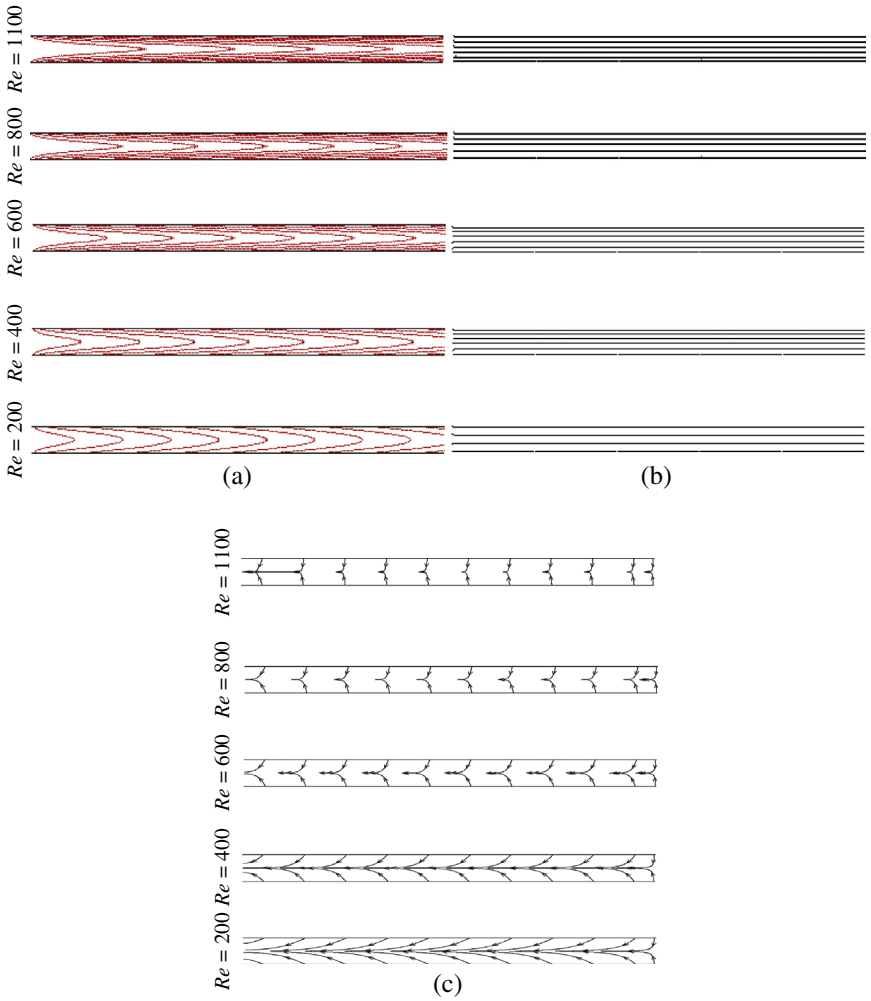

Fig. 5. Effect of *Re* on (a) temperature and (b) streamfunction and (c) heatfunction at $Pr = 6.6$.

difference $[T_i - T_a]$ profile of water with the graphical representation of Kalogirou (2004) for flat plate solar thermal collector at irradiation level 1000 W/m^2. Solar thermal collectors and applications were reported by Kalogirou (2004). Fig. 4 demonstrates the above stated comparison. As shown in Fig. 4, the numerical solutions (present work and Kalogirou (2004) are in good agreement.

4. Results and discussion

In this section, numerical results of streamlines and isotherms for various values of Reynolds number (*Re*) and Prandtl number (*Pr*) with Al_2O_3/water nanofluid in a flat plate solar collector are displayed. The considered values of *Re* and *Pr* are *Re* = (200, 400, 600, 800 and 1100), *Pr* (=4.2, 5.8, 6.6, 8.8 and 10.2) while the solid volume fraction $\phi = 5\%$. In addition, the values of the average Nusselt number, mean bulk temperature, mean sub domain velocity, percentage of collector efficiency and mid-height temperature of the riser pipe are shown graphically.

4.1. Effect of Reynolds number

The non-dimensional temperature, velocity (modulus of the velocity vector) and conductive-convective heat flux fields in terms of isothermal lines, streamlines and heatlines are displayed in Fig. 5(a–c) for the effect of Reynolds number *Re* from 200 to 1100. The strength of the thermal current activities, fluid flow and heat flux circulation are much more activated with escalating *Re*. For this Fig. 5, $Pr = 6.6$ is assumed. In the temperature distribution isothermal lines for different values of Reynolds number shows that at low value of *Re* (=200), the temperature of the nanofluid rapidly reaches to the temperature of hot walls due to low velocity. With increasing Reynolds number, increment of temperature of water–Al_2O_3 nonofluid is happened slowly, as a result the isotherms are more compressed along the riser pipe near the hot upper-lower walls and exit boundary. The thermal boundary layer thickness enhances for the greater values of inertia force.

On the other hand, in the velocity vector, initially the flow concentrates near the middle of the pipe while it

covers the whole domain of the riser pipe due to increase inertia force from 200 to 1100.

Finally, the heatlines illustrate that inertia force dominant effect plays a critical role on larger heat flow from horizontal walls to the passing fluid through the riser pipe. Heatlines also show that there is a clear difference in the heat flow trajectory for the influence of inertia force. This difference is largely attributed for $Re = 1100$ within the system. It is observed that the heatlines are not dense near the solid surfaces due to conduction dominant heat transfer. The forced convective energy transfer facilitates thermal mixing leading to high thermal gradient at the core as the dense heatlines are observed near the top and bottom walls. Deformation of heatlines near the core is observed, showing the presence of forced convection in the system. However, the thermal mixing near the core is not intense due to lower heat flow for $Re = 200$ as seen in Fig. 5c. Overall, larger heat may be recovered through the pipe for nanofluid with greater Re at $Pr = 6.6$.

4.2. Effect of Prandtl number

Fig. 6(a–c) represents the effect of Pr on the thermal, flow and heat flux fields while $Re = 400$. Isotherms are almost similar to the active parts for water-alumina nanofluid. Due to rising values of Pr, the temperature distributions become distorted resulting in an increase in the overall heat transfer. This result can be attributed to the dominance of the viscous force. It is worth noting that as the Prandtl number increases, the thickness of the thermal boundary layer near the top–bottom surfaces rises which indicates a steep temperature gradients and hence, an increase in the overall heat transfer from the hot walls to the nanofluid through the fluid passing pipe.

Fig. 6(b) describes that the streamlines occupying the whole pipe is found at the lowest value of Prandtl number ($Pr = 4.2$). Then the velocity of the water-alumina nanofluid reduces with the deviation of Pr. This happens due to fluid with greater velocity indicates lower Prandtl number. Otherwise there is no significant change in the streamfunction observed.

In the Fig. 6(c) of heatfunction, the counter clockwise and clockwise rotations of heatlines are shown via positive and negative signs of heatfunction respectively. The heatlines are seen to be connected between the top and bottom walls. Multiple flow circulations greatly influence the heatlines pattern and heat energy distributions as seen in Fig. 6 (c). Similar to the previous case, the flow clearly shows higher magnitude for heat transfer due to $Pr = 10.2$ compared to other values of Pr as seen from the heatfunction

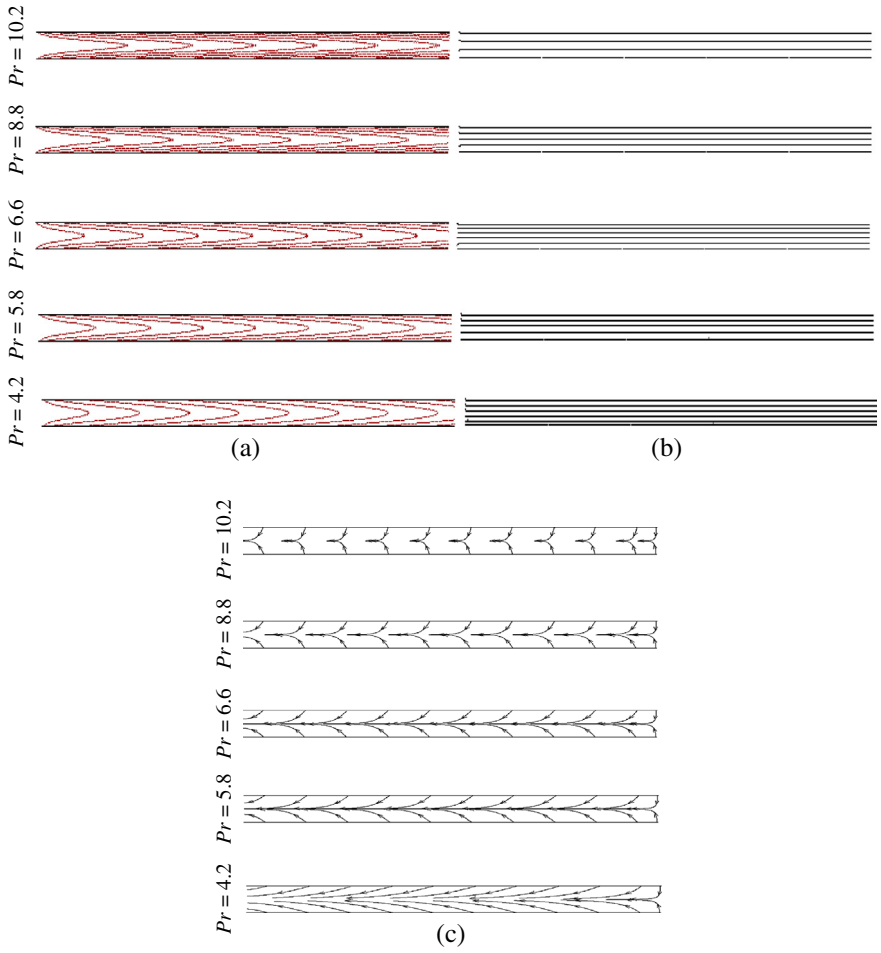

Fig. 6. Effect of Pr on (a) temperature and (b) streamfunction and (c) heatfunction at $Re = 400$.

pattern. Different viscous circulation cells are observed for heatlines near the core and this illustrates a larger magnitude of conductive heat transfer. The fluid through the riser pipe receives most of the heat from the hot walls. But, the presence of convective cells at $Pr = 4.2$ does not contribute to higher heat transfer compared to the other values of Prandtl number. Due to the growing Pr the heatlines change their shape from curved to vertical for the highest heat loss from heated surfaces to the nanofluid through the exit port of the pipe.

4.3. Rate of heat transfer

The Nu–Re and Nu–Pr profiles for water–Al_2O_3 nanofluid as well as base fluid are depicted in Fig. 7(i–ii). It is seen from Fig. 7(i) that average Nusselt number forms parabolic shape with mounting Reynolds number. The rate of forced convective heat transfer enhances 33% and 23% using nanofluid and water respectively for rising inertia force from 200 to 1100 while $Pr = 6.6$.

Fig. 7(ii) shows that Nu enhances sharply with growing Pr. The rate of heat transfer for water-alumina nanofluid is found to be more effective than the clear water due to higher thermal conductivity of solid nanoparticles. Heat transfer rate rises by 26% and 17% for nanofluid and base fluid respectively.

4.4. Mean bulk temperature

Fig. 8(i)-(ii) displays mean temperature (θ_{av}) along with the Reynolds and Prandtl numbers for both type of fluids.

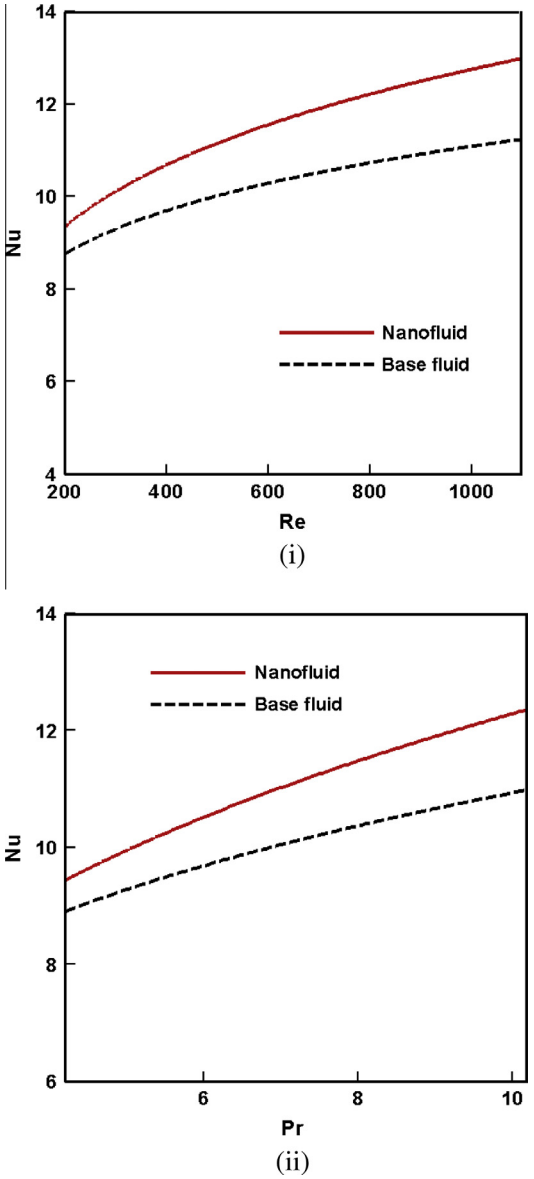

Fig. 7. Mean Nusselt number for the effect of (i) Re and (i) Pr.

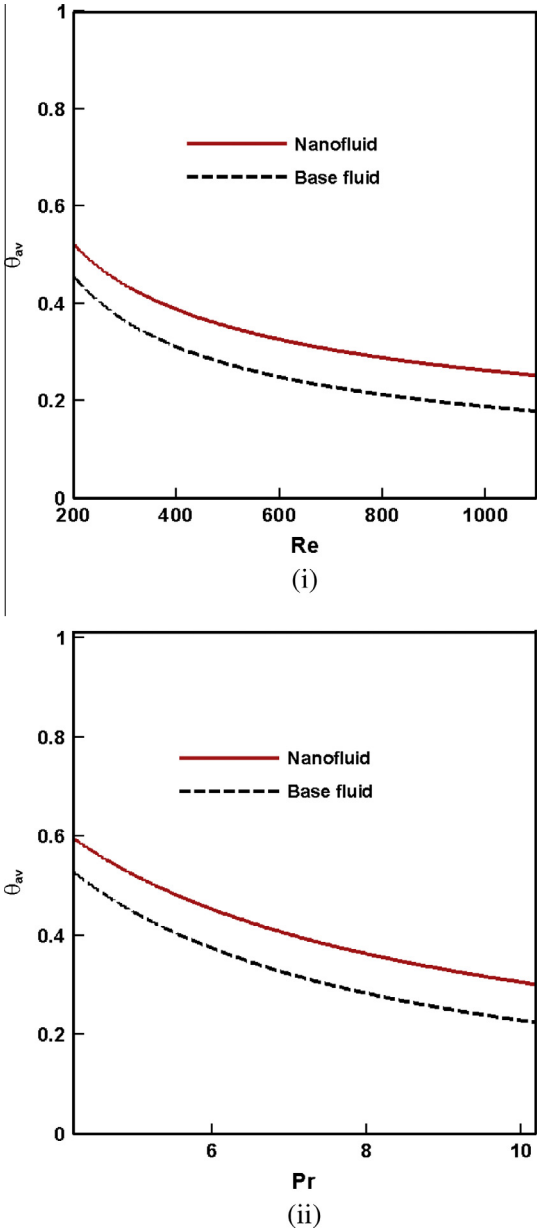

Fig. 8. Average temperature for the effect of (i) Re and (ii) Pr.

θ_{av} falls sequentially for all *Re* and *Pr*. It is well known that higher values of *Pr* indicates lower temperature of fluids. Here base fluid has lower mean temperature than the water–Al_2O_3 nanofluid.

4.5. Magnitude of average velocity

Magnitude of average velocity vector (V_{av}) for the effect of Reynolds and Prandtl numbers are expressed in the Fig. 9(i–ii). V_{av} has notable changes with different values of inertia as well as viscous forces. Clear water moves freely than solid concentrated nanofluid. Growing inertia force and falling viscous force enhance the mean velocity of the fluids through the riser pipe of the flat plate solar collector.

4.6. Collector efficiency

The variation of percentage of collector efficiency as a function of the Reynolds and Prandtl numbers varies from 200 to 1100 and 4.2 to 10.2 are exposed in Fig. 10(i–ii). It is observed from Fig. 10(i) that by introducing greater inertia force the collector efficiency increases in parabolic form. More inertia force is able to augment heat loss system through the riser pipe. In this scheme water alumina nanofluid performs better than clear water.

But rising *Pr* devalues the collector efficiency because greater *Pr* represents low tempered water which is found in winter season. So temperature of output water cannot so high as in summer season. The values of *Pr* (=4.2, 5.8, 6.6, 8.8 and 10.2) represent water of 315 K, 300 K, 295 K, 285 K and 280 K respectively.

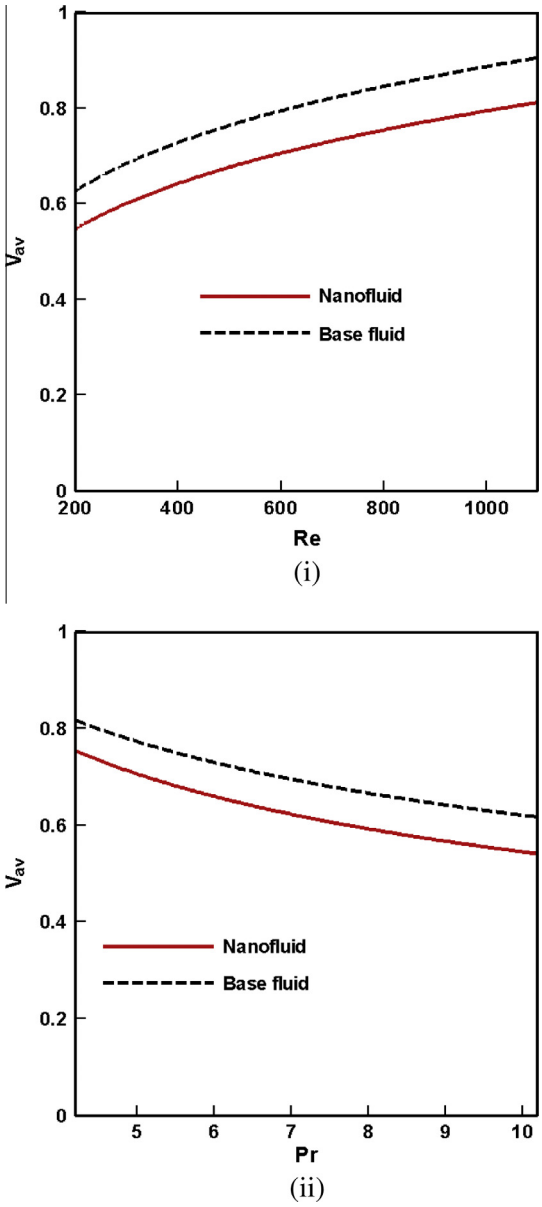

Fig. 9. Mean velocity for the effect of (i) *Re* and (ii) *Pr*.

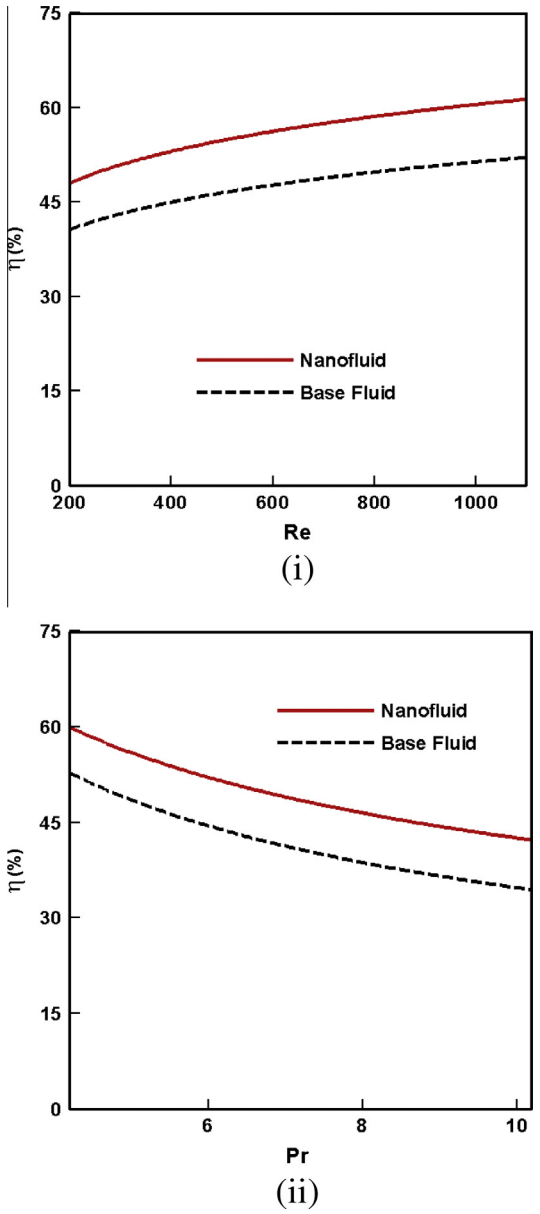

Fig. 10. Collector efficiency for the effect of (i) *Re* and (ii) *Pr*.

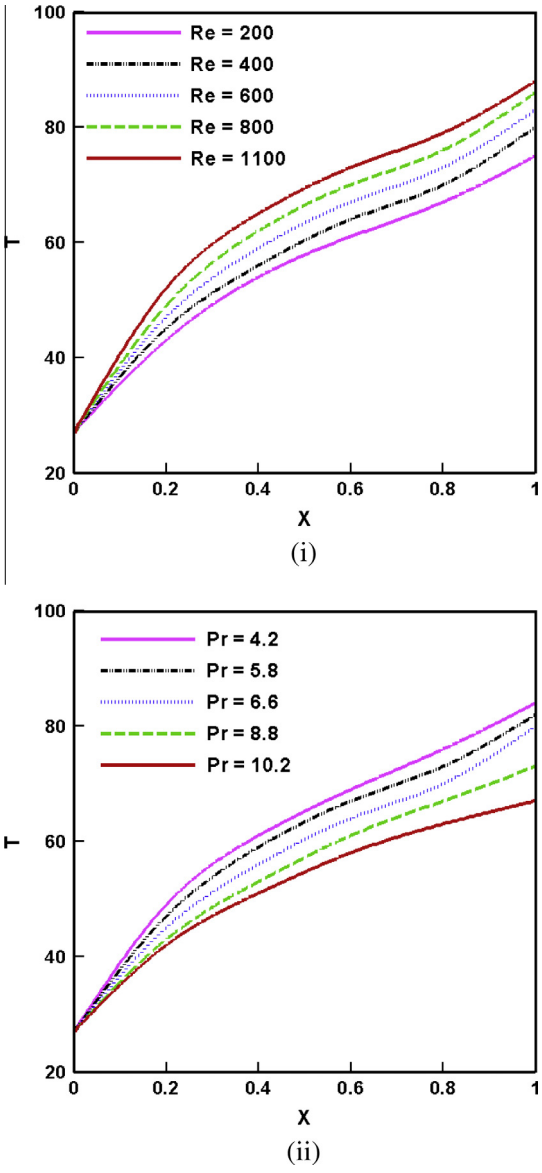

Fig. 11. Mid-height temperature for the effect of (i) *Re* and (ii) *Pr*.

Table 3
Values of *Nu* at different *Re* for the experimental, numerical and semi-empirical relation.

Re	Experimental result of Gurveer Sandhu (Sandhu, 2013) at $Pr = 7$	Numerical result at $Pr = 7$	Semi-empirical relation at $Pr = 7$
200	10.01	8.1254	9.7546
500	11.12	9.2356	11.368
800	12.021	10.0124	12.326
1100	13.10	11.2542	13.031
1400	13.511	12.0023	13.598
1700	14.012	12.5215	14.076
2000	15.00	–	–

4.7. Mid-height temperature

Fig. 11(i–ii) displays the temperature (dimensional) of water–alumina nanofluid at the middle height of the riser pipe with the influences of Reynolds and Prandtl numbers. From the Fig. 11(i) it is shown that the inlet the temperature of fluid is maintained at 300 K and then it increases gradually with the contact of heated solid upper and lower boundaries of the riser pipe. And finally the output temperature of nanofluid becomes 348 K, 353 K, 356 K, 359 K and 361 K for $Re = 200$, 400, 600, 800 and 1100 respectively.

Similarly mid-height temperature increases with growing *Pr*. The output temperature of nanofluid becomes 357 K, 355 K, 353 K, 346 K and 340 K for $Pr = 4.2$, 5.8, 6.6, 8.8 and 10.2 respectively.

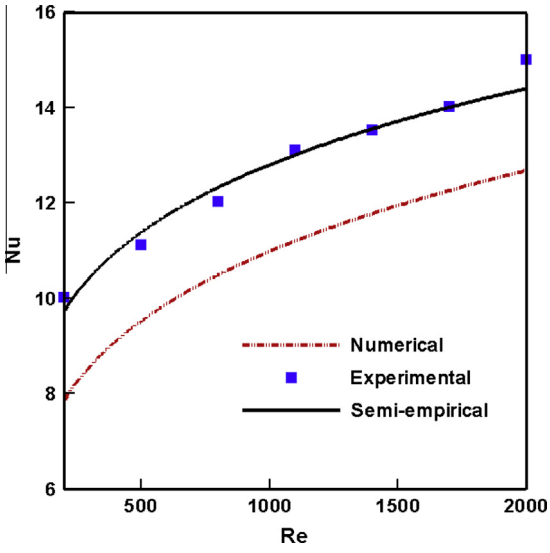

Fig. 12. *Nu–Re* profile for the experimental, numerical and semi-empirical values for water at $Pr = 7$.

5. Correlation

From the current study the calculated average Nusselt number *Nu* is correlated with Rayleigh number (*Ra*), Prandtl number (*Pr*) for base fluid (clear water) with $4.2 \leqslant Pr \leqslant 10.2$, $200 \leqslant Re \leqslant 1700$ through the riser pipe of the horizontal flat plate solar collector. This correlation can be written as

$$Nu = (0.9223 + 0.2327Pr)(Re)^{0.2120} \quad (19)$$

The confidence coefficient is $R^2 = 97.03\%$.

5.1. Semi-empirical relation

A semi-empirical relation is established from the correlation of the Eq. (18) with the experimental data provided by Sandhu (2013) which can be written as

$$Nu = 2.2275 + (0.8849 + 0.2233Pr)(Re)^{0.2120} \quad (20)$$

5.2. Comparison with experimental result

The present results are compared with the experimental results available in the literature. Table 3 provides the

values of average Nusselt number from the experimental result as Sandhu (20130, the numerical results from Eq. (18) and the semi-empirical result as in Eq. (19). Value of $Pr = 7$ is used in Eq. (18) and Eq. (19). In Fig. 12 the graphical representation of the average Nusselt number (Nu) corresponding to Table 3 has been shown. This figure demonstrates a good agreement between the experimental result and that obtained by the semi-empirical relation from the current Study.

6. Conclusion

The influences of Reynolds number and Prandtl number on forced convection boundary layer flow inside the riser pipe of a flat plate solar collector with water–Al_2O_3 nanofluid are accounted. Various Re and Pr have been considered for the temperature, flow and heat flux fields as well as heat transfer rate, mean bulk temperature, average velocity, collector efficiency and mid-height temperature of the fluids through the riser pipe. The results of the numerical analysis lead to the following conclusions:

- The structure of the fluid isotherms, streamlines and heatlines through the solar collector is found to significantly depend upon the Re and Pr.
- The Al_2O_3 nanoparticles with the highest Re and Pr are established to be most effective in enhancing performance of heat loss rate than base fluid.
- Collector efficiency is obtained higher for rising Re and falling Pr.
- Mean temperature diminishes for both fluids with rising both parameters.
- Average velocity field increases due to growing Re and diminishing Pr.

References

Álvarez, A., Muñiz, M.C., Varela, L.M., Cabeza, O., 2010. Finite element modelling of a solar collector, Int. Conf. on Renew. Energies and Power Quality, Granada (Spain).

Amrutkar, S.K., Ghodke, S., Patil, K.N., 2012. Solar flat plate collector analysis. IOSR J. Eng. 2 (2), 207–213.

Azad, E. Interconnected heat pipe solar collector, IJE Transactions A: Basics, Vol. 22, No. 3, September 2009–233.

Chabane, F., Moummi, N., Benramache, S., Bensahal, D., Belahssen, O., Lemmadi, F.Z., 2013. Thermal performance optimization of a flat plate solar air heater. Int. J. Energy Tech. 5 (8), 1–6.

Dara, J.E. Ikebudu, K.O., Ubani, N.O., Chinwuko, C.E., Ubachukwu, O.A., 2013. Evaluation of a passive flat-plate solar collector, Int. J. Adv. Res. Tech. 2 (1).

Dechaumphai, P., 1999. Finite Element Method in Engineering, 2nd ed. Chulalongkorn University Press, Bangkok.

Iordanou, G. Flat-plate solar collectors for water heating with improved heat transfer for application in climatic conditions of the mediterranean region, Doctoral thesis, Durham University, 2009.

Kalogirou, Soteris A., 2004. Solar thermal collectors and applications. Prog. Energy Combust. Sci. 30, 231–295.

Karanth, K.V., Manjunath, M.S., Sharma, N.Y., 2011. Numerical simulation of a solar flat plate collector using discrete transfer radiation model (DTRM)–a CFD approach, Proc. of the World Congress on Engg. 2011, Vol III, WCE 2011, London, U.K.

Karuppa, R.R.T.K., Pavan, P., Rajeev, D.R., 2012. Experimental investigation of a new solar flat plate collector. Res. J. Eng. Sci. 1 (4), 1–8.

Kazeminejad, H., 2002. Numerical analysis of two dimensional parallel flow flat-plate solar collector. Renew. Energy 26, 309–323.

Kolb, A., Winter, E.R.F., Viskanta, R., 1999. Experimental studies on a solar air collector with metal matrix absorber. Solar Energy 65 (2), 91–98.

Lambert, A.A., Cuevas, S., del Río, J.A., 2006. Enhanced heat transfer using oscillatory flows in solar collectors. Solar Energy 80, 1296–1302.

Lund, K.O., 1986. General thermal analysis of parallel-flow flat-plate solar collector absorbers. Solar Energy 5, 443.

Mahian, O., Kianifar, A., Kalogirou, S.A., Pop, I., Wongwises, S., 2013. A review of the applications of nanofluids in solar energy. Int. J. Heat Mass Trans. 57, 582–594.

Martín, R.H., Pinar, A.G., García, J.P., 2011. Experimental heat transfer research in enhanced flat-plate solar collectors. In: Solar Thermal Applications, World, Renewable Energy Congress-2011, pp. 3844–3851.

Maxwell-Garnett, J.C., 1904. Colours in metal glasses and in metallic films. Philos. Trans. Roy. Soc. A 203, 385–420.

Moningi, M.K., 2009. Conduction convection radiation processes of a solar collector using FEA. University of Massachusetts, Amherst.

Nag, A., Misra, D., De, K.E., Bhattacharya, A., Saha, S.K., 1989. Parametric study of parallel flow flat plate solar collector using finite element method, In: Num. Methods in Therm. Problems, Proc. of the 6th Int. Conf., Swansea, UK.

Natarajan, E., Sathish, R., 2009. Role of nanofluids in solar water heater. Int J Adv Manuf. Technol.. http://dx.doi.org/10.1007/s00170-008-1876-8.

Ogut, E.B., 2009. Natural convection of water-based nanofluids in an inclined enclosure with a heat source. Int. J. Therm. Sci. 48 (11), 2063–2073.

Otanicar, T.P., Phelan, P.E., Prasher, R.S., Rosengarten, G., Taylor, R.A., 2010. Nanofluid-based direct absorption solar collector. J. Renew. Sust. Energy 2, 033102.

Pak, B.C., Cho, Y., 1998. Hydrodynamic and heat transfer study of dispersed fluids with submicron metallic oxide particle. Exp. Heat Transfer 11, 151–170.

Piao, Y., Hauptmann, E.G., Iqbal, M., 1994. Forced convective heat transfer in cross-corrugated solar air heaters. ASME J. Solar Energy Eng. 116, 212–214.

Polvongsri, S., Kiatsiriroat, T., 2011. Enhancement of Flat-Plate Solar Collector Thermal Performance with Silver Nano-fluid, The 2nd TSME Int. Conf. on Mech. Engg. 2011, Krabi.

Reddy, J.N., Gartling, D.K., 1994. The Finite Element Method in Heat Transfer and Fluid Dynamics. CRC Press Inc, Boca Raton, Florida.

Saleh, A.M., 2012. Modeling of flat-plate solar collector operation in transient states, thesis of Master of Sci. in Engg., 2012, Purdue University, Fort Wayne, Indiana.

Saleh, H., Roslan, R., Hashim, I., 2011. Natural convection heat transfer in a nanofluid-filled trapezoidal enclosure. Int. J. Heat Mass Trans. 54, 194–201.

Sandhu, G., 2013. Experimental study of temperature field in flat-plate collector and heat transfer enhancement with the use of insert devices, M. of Engg. Sci. thesis, The School of Graduate and Postdoctoral Studies, The University of Western Ontario London, Ontario, Canada.

Struckmann, F., 2008. Analysis of a Flat-plate Solar Collector, Project Report 2008 MVK160 Heat and Mass Transport, 2008, Lund, Sweden.

Taylor, C., Hood, P., 1973. A numerical solution of the Navier-Stokes equations using finite element technique. Comput. Fluids 1, 73–89.

Taylor, R.A., Phelan, P.E., Otanicar, T.P., Adrian, R., Prasher, R., 2011. Nanofluid optical property characterization: towards efficient direct absorption solar collectors. Nanoscale Res. Lett. 6, 225.

Tripanagnostopoulos, Y., Souliotis, M., Nousia, T., 2000. Solar collectors with colored absorbers. Solar Energy 68, 343–356.

Tyagi, H., Phelan, P., Prasher, R., 2009. Predicted efficiency of a low-temperature nanofluid-based direct absorption solar collector. J. Solar Energy Eng. 131, 041004-1.

Zambolin, E. Theoretical and experimental study of solar thermal collector systems and components, Scuola di Dottorato di Ricerca in Ingegneria Industriale, Indirizzo Fisica Tecnica.